Ocean Engineering 90 (2014) 39–48

Contents lists available at ScienceDirect

Ocean Engineering

journal homepage: www.elsevier.com/locate/oceaneng

Kite and classical rig sailing performance comparison on a one design keel boat

R. Leloup [a,b], K. Roncin [b,*], G. Bles [b], J.-B. Leroux [b], C. Jochum [b], Y. Parlier [a]

[a] OCEA, rue des Terres Neuves, BP 21, 33322 Bègles Cedex, France
[b] Mechanics of Naval Structures, LBMS (EA 4325) ENSTA Bretagne, 2 rue François Verny, 29806 Brest, France

ARTICLE INFO

Article history:
Received 15 November 2013
Accepted 27 June 2014
Available online 8 August 2014

Keywords:
Dynamic simulation
Wind energy
Kite
Kiteboat
Sailboat
Velocity prediction programme

ABSTRACT

An implementation of a kite modelling approach into 6 degrees of freedom sailboat dynamic simulator is introduced. This enables an evaluation of kite performance in comparison with classical rig sailing.

A zero-mass model was used to model kite forces. Influence of the wind gradient was properly taken into account leading to significant modifications in the calculation of the relative wind. The modelling was performed with experimental aerodynamic characteristics. An optimization was done to determine the best kite flight trajectory in terms of performance.

Validation steps of the sail yacht simulator were performed for a classical rig on the example of an 8 m one design yacht. The experimental set-up is described and validation results are discussed. Particularly, a wind mesh was used, based on measurements made at four different locations of the navigation spot. Additionally boat motions were recorded by high resolution GPS and inertial unit systems.

Speed polar diagram results, reached by kite propulsion, were predicted versus true wind angle. At last a comparison was made for upwind and downwind legs in sea trials conditions, between simulations with the classical rig and the kite. It is shown that the boat towed by kite would achieve much better sailing performance.

1. Introduction

Regarding world speed records, kite surfers demonstrated the performance efficiency of kites. In this context, taking advantage of wind using kites as propulsion systems for yachts can be an alternative to conventional sails. This study takes place within the project “beyond the sea®” launched by Yves Parlier and is managed in partnership with the LBMS laboratory of ENSTA Bretagne and the French ministry of defence.

A methodology for kite propulsion efficiency analysis regarding a classical rig sailing yacht is presented in this paper. The aim of the paper is to assess the benefits of the kite rig used for propulsion compared to the classical rig. In this framework, regarding the lack of data for the validation of kite rig propulsion models, the leading idea of the paper is to consider on one hand a VPP basis validated on a classical rig by sea trials and on the other hand, existing experimental aerodynamic properties of a flying kite (Dadd et al., 2010). Thus, replacing the classical rig part in the VPP scheme by the one, dedicated to the kite rig and using experimental aerodynamic coefficients, can reasonably be considered as a first predictive step for kite rig benefits. Of course, the next step should be the comparison of the kite benefits prediction with measurements. Consequently differences between the two propulsion technologies applied to the same yacht are highlighted and discussed. One of the first studies on kites and their ability to produce energy was achieved by Loyd (1980). More recently, the literature provides numerous articles which started to treat flight dynamics (de Groot, 2010; Terink, 2009), flight control (Fagiano, 2009), structure deformation (Breukels, 2011), or aerodynamic forces modelling (Maneia, 2007; de Wachter, 2008).

Despite very fine approaches have been achieved in order to model the kite's flight applying Newton's laws (Terink, 2009; Breukels, 2011) even taking into account kite's lines and mass distribution like de Groot (2010), the so-called zero-mass model (Wellicome and Wilkinson, 1984) remains well known and widely used as its simplicity makes it easy to connect with. Within this model, Newton's laws are applied considering only the aerodynamic resultant and tethers tensions, since the mass of the kite is neglected. Even recently, numerous studies dealing with flight strategies optimization for boat propulsion such as Wellicome and Wilkinson (1984), Naaijen et al. (2006, 2010), Dadd (2013) or with

* Corresponding author. Tel.: +33 2 98348748; fax: +33 2 98348730.
E-mail address: kostia.roncin@ensta-bretagne.fr (K. Roncin).
URL: http://www.parlier.org (Y. Parlier).

http://dx.doi.org/10.1016/j.oceaneng.2014.06.043
0029-8018/

Nomenclature

Notation – parameter (unit)

A_k	kite surface (m^2)
C_D	drag coefficient of the kite (dimensionless)
C_L	lift coefficient of the kite (dimensionless)
$\mathbf{D}$	kite drag vector (N)
D	kite drag magnitude (N)
$\mathbf{F}_a$	aerodynamic resultant vector (N)
F_a	aerodynamic resultant magnitude (N)
l_T	tethers length (m)
$\mathbf{L}$	kite lift vector (N)
L	kite lift magnitude (N)
n	coefficient which is equal to 1/7 for the sea surface according to ITTC (2011) (dimensionless)
$\mathbf{T}$	tethers tension vector (N)
T	tethers tension magnitude (N)
$\mathbf{U}_{10}$	true wind velocity vector at standard altitude (10 m) ($m\,s^{-1}$)
U_{10}	true wind velocity magnitude at standard altitude (10 m) ($m\,s^{-1}$)
$\mathbf{V}_a$	kite apparent wind velocity vector ($m\,s^{-1}$)
V_a	kite apparent wind velocity magnitude ($m\,s^{-1}$)
$\mathbf{V}_k$	kite velocity vector ($m\,s^{-1}$)
V_k	kite velocity magnitude ($m\,s^{-1}$)
$\mathbf{V}_s$	ship velocity vector ($m\,s^{-1}$)
V_s	ship velocity magnitude ($m\,s^{-1}$)
$\mathbf{V}_{WR}$	relative wind velocity vector at kite altitude (relative to boat course) ($m\,s^{-1}$)
V_{WR}	relative wind velocity magnitude at kite altitude (relative to boat course) ($m\,s^{-1}$)
$\mathbf{V}_{WT}$	true wind velocity vector ($m\,s^{-1}$)
V_{WT}	true wind velocity magnitude ($m\,s^{-1}$)
z	altitude above sea level (m)
$\alpha_{geom.}$	geometric incidence (rad)
β_{WT}	true wind angle (relative to boat course) (rad)
β_{WR}	relative wind angle at kite altitude (relative to boat course) (rad)
χ_{vk}	kite velocity angle (rad)
ε	kite lift to drag angle (rad)
θ	elevation angle (rad)
ρ_{air}	air density ($kg\,m^{-3}$)
ϕ	azimuth angle (rad)

Reference frames

R_F ($O,\mathbf{x}_F,\mathbf{y}_F,\mathbf{z}_F$)	ship velocity reference frame
R_{WT} ($O,\mathbf{x}_{WT},\mathbf{y}_{WT},\mathbf{z}_{WT}$)	true wind reference frame
R_{WR} ($A,\mathbf{x}_{WR},\mathbf{y}_{WR},\mathbf{z}_{WR}$)	relative wind at kite altitude reference frame
R_{k0} ($K,\mathbf{x}_{k0},\mathbf{y}_{k0},\mathbf{z}_{k0}$)	kite position reference frame
R_a ($K,\mathbf{x}_a,\mathbf{y}_a,\mathbf{z}_a$)	aerodynamic reference frame
R_b ($K,\mathbf{x}_b,\mathbf{y}_b,\mathbf{z}_b$)	body reference frame
$\mathbf{x}_{vk}$	kite velocity direction unit vector

real-time control for kites such as Erhard and Strauch (2013a)) or Costello et al. (2013), rely on this kind of zero-mass approach. In fact, its very low computational cost and its reasonable predictions regarding experiments balance out its high level of approximation. As few examples Wellicome and Wilkinson (1984) can be cited as they compared stationary and dynamic flight strategies applying them for boat propulsion. Dadd et al. (2010, 2011) studied dynamic flight with 8-shaped trajectories and obtained rather satisfactory comparisons with experimental measurements. Furthermore, Naaijen et al. (2006, 2010) developed a performance prediction programme dedicated to a merchant ship to assess fuel saving capabilities of a kite. The present study is inspired from previous works (Leloup, 2013a) which integrated an aerodynamic kite model within the zero mass model. This model also allowed to predict fuel saving on a 60,000 dwt tanker (Leloup et al., 2013b).

The modelling approach for a flying kite is presented in the first part of the study. The wind gradient linked to atmospheric boundary layer is taken into account, and analytical expressions for apparent wind velocity seen by the kite and for kite velocity at each position within the wind window are presented. An optimization technique for the best flight configuration is then proposed. Especially, this optimization technique differs from the literature (Naaijen et al., 2006), namely by the analysis of vertical 8-shaped trajectories (Dadd, 2011) which enable significant upwind benefits, as shown in Section 4. At last, to ensure the use of real validated data, kite aerodynamic parameters were taken from Dadd experiments (Dadd et al., 2010, 2011). In the second part of the study, the kite modelling approach was implemented into a dynamic velocity prediction programme (DVPP) (Roncin and Kobus, 2004) for an 8 m one design yacht, the Beneteau First Class 8. Validity of the DVPP was assessed by sea trials comparisons that are presented and discussed. The comparison between classical rig and kite propulsion is presented and discussed in the two last sections, based on velocity polar diagrams and on upwind and downwind legs.

2. Modelling approach of a flying kite

This section presents the setting technique used to describe the kite within the flying window. This enables kite velocities descriptions which are the main input data for the velocity comparison strategy with a classical sailing rig presented in this study.

2.1. Wind window reference frames

An illustration of the kite within the half sphere wind window, which is bounded by the wind window edge, is shown in Fig. 1. In this figure O denotes the attachment point of the tethers to a reference point (ground or deck of a ship for instance, here we take the centre of gravity of the boat).

In case of a boat, the wind window is oriented by the relative wind velocity vector $\mathbf{V}_{WR}$ at each point. Pay attention to the fact

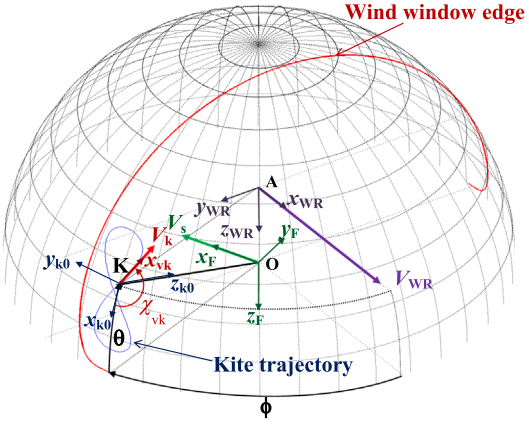

Fig. 1. Flying kite within the wind window. (For interpretation of the references to color in this figure, the reader is referred to the web version of this article.)

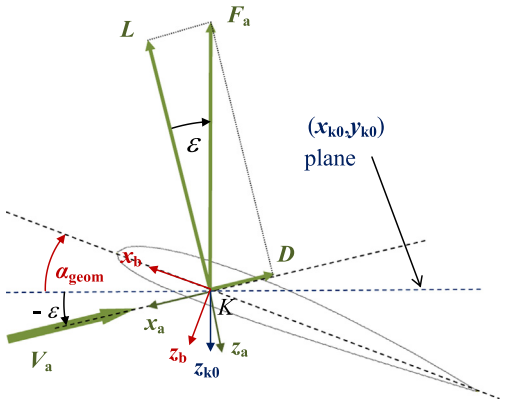

Fig. 2. Aerodynamic forces vector decomposition in the kite symmetry plane.

that relative wind is used to be called apparent wind for the sailing boat. The notation adopted here is the ITTC Standard notation (ITTC, 2011) that allows, in the case of kite, to clearly distinguish the relative wind seen by the boat and the apparent wind seen by the kite. The kite is represented Fig. 1 by point *K*, which is located at the quarter chord in the symmetry plane of the kite. The reference frame R_{k0}, which is attached to point *K*, is obtained by rotating about $\mathbf{z}_{WR}$ by the azimuth angle ϕ, and then by the elevation angle $(\theta-\pi/2)$ around $\mathbf{y}_{k0}$. Unit vector $\mathbf{x}_{vk}$ is oriented along the direction of the kite velocity and is obtained by rotating vector $\mathbf{x}_{k0}$ about $\mathbf{z}_{k0}$ by angle χ_{vk}. R_b is the body reference frame, attached to the kite as presented in Fig. 2. The aerodynamic reference frame R_a is oriented in accordance with the kite apparent wind velocity $\boldsymbol{V}_a$. Reference frame R_F is fixed in relation to the flow so that $\mathbf{x}_F$ axis is in the course direction along the ship velocity $\mathbf{V}_s$.

However, tethers length can usually be around several hundred metres to facilitate high wind capture. This makes sense to take wind gradients effects with altitude into account.

2.2. Wind gradient description

The wind friction with the sea surface (or ground) leads to a zero wind velocity at sea level. Therefore the true wind velocity V_{WT} decreases when altitude decreases. This phenomenon is called wind gradient and was introduced in the modelling as a function of altitude instead of a constant wind velocity. According to ITTC (2011), the wind velocity as a function of altitude can be calculated using the formula:

$$V_{WT} = U_{10}(z/10)^n \tag{1}$$

where U_{10} is the wind velocity at standard altitude 10 m ($m\,s^{-1}$), z is altitude above sea level (m). n is a coefficient which is equal to 1/7 for the sea surface according to ITTC (2011).

The wind velocity according to altitude is plotted in Fig. 3. One can see that the wind velocity increases when altitude increases. Therefore, it can be more favourable to use a kite which flies at high altitude where the wind velocity is higher.

2.3. Kite velocity based on the zero mass modelling approach

This section presents a review made on the common zero mass model (Dadd et al., 2010, 2011; Wellicome and Wilkinson, 1984). It was partly described in a previous work (Leloup, 2013a).

According to Newton's laws applied to the kite at point *K*, assuming that the mass of the kite is neglected, equilibrium equation is as follows:

$$\mathbf{T}+\mathbf{F}_a=\mathbf{0} \tag{2}$$

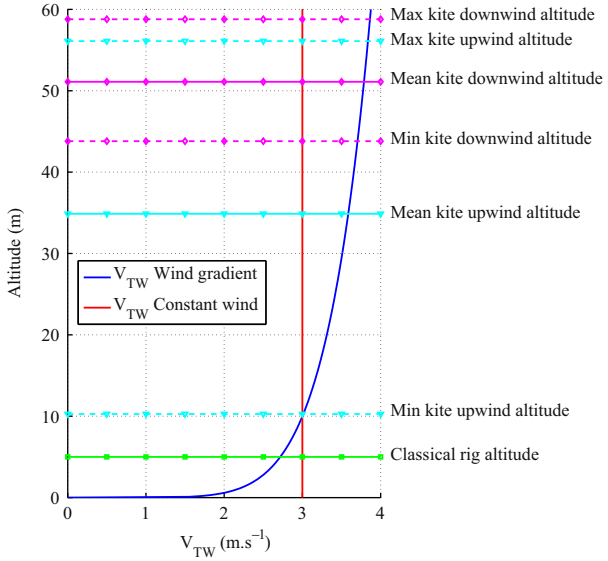

Fig. 3. Wind velocity according to altitude.

The aerodynamic resultant, $\mathbf{F}_a$, compensates the tethers tension, **T**, at any time and these two forces are aligned on the same axis that goes from attachment point O to the point K of the kite. The second equation which governs the kite motion is the apparent wind equation:

$$\mathbf{V}_a=\mathbf{V}_{WR}-\mathbf{V}_k \tag{3}$$

with $\mathbf{V}_{WR}=\mathbf{V}_{WT}-\mathbf{V}_s$, where $\mathbf{V}_s$ denotes the ship velocity.

According to the definition of the aerodynamic resultant, we have

$$\mathbf{F}_a=\mathbf{L}+\mathbf{D} \tag{4}$$

The apparent wind velocity vector $\mathbf{V}_a$ is assumed to remain in the symmetry plane of the kite. This leads in the plane $(\mathbf{x}_a,\mathbf{z}_a)$, to the configuration shown in Fig. 2. As demonstrated by Leloup et al. (2012, 2013a) the projection of Eq. (3) onto the corresponding axes and by scalar product with $\mathbf{z}_{k0}$:

$$V_a=-\frac{V_{WR}\mathbf{x}_{WR}.\mathbf{z}_{k0}}{\sin\,\varepsilon} \tag{5}$$

Moreover, using the scalar product properties, Eq. (3) leads to

$$|\mathbf{V}_a|^2=|\mathbf{V}_{WR}|^2+|\mathbf{V}_k|^2-2|\mathbf{V}_{WR}||\mathbf{V}_k|(\mathbf{x}_{WR}.\mathbf{x}_{vk}) \tag{6}$$

Combined with Eq. (5), Eq. (6) can be seen as a second order equation of the velocity of the kite V_k leading therefore to

$$V_k=V_{WR}\left[\mathbf{x}_{WR}.\mathbf{x}_{vk}+\sqrt{(\mathbf{x}_{WR}.\mathbf{x}_{vk})^2+\left(\frac{\mathbf{x}_{WR}.\mathbf{z}_{k0}}{\sin\,\varepsilon}\right)^2-1}\right] \tag{7}$$

The velocity of the kite is real only if

$$|\mathbf{x}_{WR}.\mathbf{x}_{vk}|\geq\sqrt{\left|1-\left(\frac{\mathbf{x}_{WR}.\mathbf{z}_{k0}}{\sin\,\varepsilon}\right)^2\right|} \tag{8}$$

Condition (8) shows that the existence of the velocity of the kite is only defined for a given flying area so-called manoeuvrable area below the red limit line shown in Fig. 1. In this area the kite can move in all directions. Above the red limit line, the kite cannot fly. It corresponds to the wind window edge.

2.4. Aerodynamic characteristics

A sail area of 35 m² was used during sea trials with a one design sailboat settled with a classical rig. For didactical reasons, the same area of 35 m² as for the classical rig in upwind conditions was

taken for the kite. This is an arbitrary choice since results strongly depend on kite area considered. But on the other hand, additional spinnaker area in downwind conditions was not added to the kite area. Nevertheless, a 35 m² kite appears to be still manageable on a boat as demonstrated by the *kiteboat* project. To have as much as possible an accurate and realistic aerodynamic description of the kite rig, data provided by Dadd experiments, performed on a Flexifoil blade III ram-air kite, were considered to be accurate enough to be set in the VPP scheme. Thus, the lift coefficient C_L and glide angle ε are 0.776 and 9.55 ° (lift to drag ratio 5.94) respectively (Dadd et al., 2010). These aerodynamic parameters are the same for static and dynamic flight. Moreover, they remain constant along a flight trajectory.

However, the question of tether length has also to be addressed since increasing tethers length might also delay control command requests. Nonetheless Bosch et al. (2014) indicated that below 100 m tether length there is no control issue. This is confirmed by the *kiteboat* project where 80 m tether length was used for the trials. Accordingly, a typical tethers length of 100 m was considered in a first approach.

2.5. Propulsive force generated by the kite

Once apparent wind velocity of the kite V_a is known at each position within the wind window, the tethers tension resultant **T**, which is opposite to the aerodynamic resultant $\mathbf{F}_a$ according to Eq. (2), can be expressed as follows:

$$T = \frac{1}{2}\frac{C_L \rho_{air} A_k V_a^2}{\cos\ \varepsilon}\mathbf{z}_{k0} \tag{9}$$

The projection of the tethers tension onto the axis $\mathbf{x}_F$, directly gives the propulsive force generated by the kite. It depends on the relative wind angle β_{WR} (relative to ship course) at kite altitude as presented in Fig. 4. Projecting on the $\mathbf{y}_F$ axis, we obtain the drift force. These forces are integrated with respect to time along the flight trajectory of the kite, in order to obtain their average values for a given trajectory. This enables comparison of the trajectories efficiency based on average propulsive force.

As shown in Fig. 4, true wind velocity V_{WT} variation with altitude modifies the relative wind angle β_{WR} observed at 10 m (ship level for instance). The orientation of the wind window is therefore varying with the altitude, leading to a twist of the wind window edge which is no more a circle, as shown in Fig. 1. Especially, it is pointed out that the wind window orientation is modified with increasing altitude. The wind window is oriented by the relative wind angle β_{WR} at the altitude of the kite. As the kite altitude increases, the relative wind angle β_{WR} progressively increases as well, leading therefore to more efficient towing force in direction. This is a key point that has to be considered for kite propulsive force optimization strategy presented in the next section.

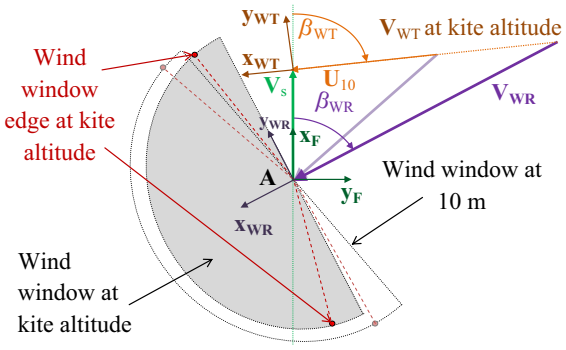

Fig. 4. Kite flying wind window 10 m above sea level and at a given altitude higher than 10 m.

2.6. Maximum propulsive force polar algorithm

For a given ship and true wind velocity, the polar plot of the maximum propulsive force can be done according to the true wind angle β_{WT} relative to ship course. For each β_{WT} value a kite flight optimization loop was developed testing, for given elevation angles θ of the kite, both static and dynamic flight cases.

In case of a static flight, for a given elevation angle θ, the azimuth angle ϕ was computed in order to put the kite on the wind window edge which is the only location to keep the kite into a static position according to condition (8). According to Fig. 1, the azimuth angle ϕ can be expressed as follows:

$$\cos\ \phi = \pm\frac{\sin\ \varepsilon}{\cos\ \theta} \tag{10}$$

This leads to two solutions, one positive and the other negative, which only one can be retained as propulsive.

The dynamic flight case was investigated for an 8-shaped trajectory which is the most common trajectory applied to kite flights avoiding tethers to get tangled. The most commonly used mathematical expressions of an 8-shaped trajectory are given by Argatov et al. (2009) and Wellicome and Wilkinson (1984). Argatov et al. trajectory definition was chosen in this study since it is much simpler than Wellicome and Wilkinson trajectory.

The size of the trajectory can be modified thanks to azimuth and elevation amplitude parameters. In the scope of the zero-mass model assumptions, the trajectory size reduction (azimuth and elevation amplitude decrease) enhances trajectory efficiency from a propulsive force point of view. Nevertheless, Dadd (2013) explains that "[…] the practical minimum limits for these are not known". Therefore a reasonable trajectory size was used in this study (azimuth amplitude: 30°, elevation amplitude 10°).

At a given elevation, a variation of the azimuth angle of the trajectory was conducted in order to grasp the best average propulsive force obtained during one period of the flight. Indeed, the best azimuth positioning of the trajectory appears to be a compromise between maximal tension zone (azimuth equal to 0°) of the wind window and the vessel motion direction. Moreover, if the tether tension projection onto the vessel axis $\mathbf{x}_F$ is negative, it denotes a negative propulsive force. Thus, useful wind window would be smaller as relative wind angle β_{WR} decreases.

The last control parameter which can be modified in the present study is the trajectory orientation (horizontal or vertical). This parameter was added to Naaijen et al. (2006) approach to improve the dynamic flight performance of the kite. The best trajectory azimuth was calculated for an horizontal and a vertical trajectory. This loop is done up to the maximum elevation for the two trajectories.

At the end of the whole optimization loop, comparison between maximum static and dynamic (vertical and horizontal trajectories) propulsive forces is finally done, and the best configuration is retained. Corresponding ship transverse and vertical components of the tethers tension can be deduced.

3. Yacht dynamic simulations set-up

The dynamic velocity prediction programme set by Roncin (Roncin and Kobus, 2004) was used for dynamic simulations with a kite rig. Nevertheless, a validation of the dynamic velocity prediction programme was first performed with a classical rig and compared to sailing yacht measurements. Consequently experimental set-up and corresponding validation is presented

and discussed in this section. The boat is an 8 m one design, the Beneteau First Class 8 whose characteristics are

- LOA: 8.5 m
- Beam: 2.49 m
- Draught: 0.7–1.75 m
- Displacement: 1.400 t
- Upwind sails surface: 34 m²
- Downwind sails surface: 65 m²

Hydrodynamic forces were deduced from towing tank extensive test studies performed with the design of experiment method principle. The aerodynamic model for the classical rig developed by Claughton (1999) was considered. Claughton took also the waves into account and his formulation was used to calculate the added resistance in waves.

3.1. Experimental set-up

The validation of the simulator was performed by sea trials conducted in collaboration with the Centrale Nantes (ECN) graduate school of engineering, the French national school of sailing (ENV) and the University for applied Technology on the Nantes campus (Roncin et al., 2005).

3.1.1. Yacht positioning data

The boat and the measurement system can be seen in Fig. 5. Speed and position were measured by a high resolution GPS DG16 from Thales, which give accuracy below the metre. Rudder angle was measured by a potentiometer. Attitude and rates in rotation are given by an inertial unit from Xsens provided by the Cadden Company. All data feed the central unit to be synchronized and stored in memory. All data are transmitted in live to a base onshore by the mean of an Ultra High Frequency signal.

3.1.2. Wind measurements

The wind was measured by ultra-sonic wind vane CV3F by LCJ sensors. This kind of technology guarantees a good independence between wind measurement and platform motions. Four wind sensors were set around the sailing area on fixed KL15 catamarans. This enables a mesh of the wind field that covers all the sailing area as shown in Fig. 6.

The wind at boat location was obtained from a simple linear interpolation in time and space. This technique takes advantage from a simple wind vane settled on the boat since it is far less disturbed by the air flow deviation around the sails or by the motions of the boat or the deformation of the mast and rig. Relative wind angle is deduced from the wind interpolation at boat location and from the boat speed given by the GPS measurements. Note that sea current was taken into account from public data provided by the SHOM, (French hydrography and oceanography service), and was interpolated in time. Wind interpolation was validated by comparison between measured wind and predicted wind done for one of the four sensors thanks to data provided by the three others. Results displayed in Fig. 7 are almost satisfying since the observed differences are mostly below sensors accuracy.

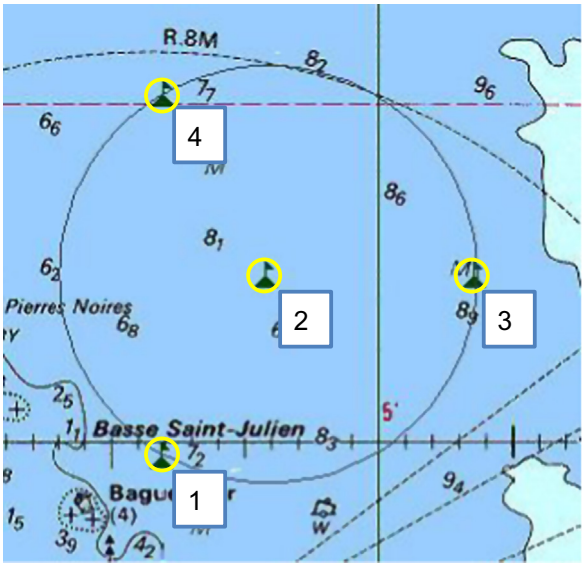

Fig. 6. Example of KL 15 wind sensors platform location for wind field meshing.

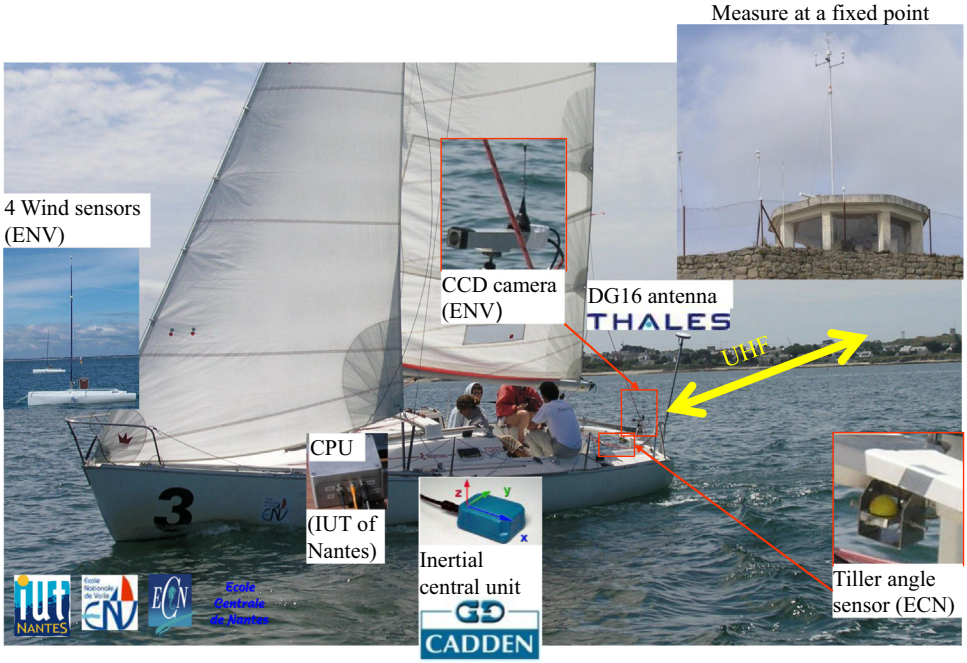

Fig. 5. Sea trials on the 8 m one design yacht.

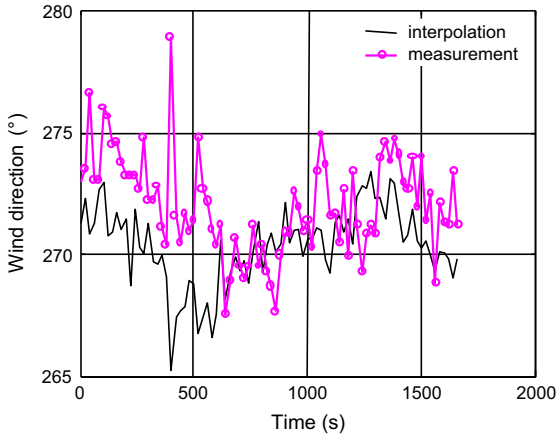

Fig. 7. Example of interpolated wind direction compared with experimental wind measure, for the same location.

The same interpolation technique was conducted for wind velocity. A relative gap of 13% was found between measurements and interpolation results which is reasonably satisfying at this stage.

3.1.3. Main uncertainties

A rigorous and exhaustive uncertainty analysis still remains an open question in the case of full scale trials in real conditions. Even if all set-up devices precisions were known, standard statistical analysis of repeated trials could not be achieved properly, since the whole experimental environment could not be entirely known and controlled. Nevertheless, this section provides the uncertainties which could have been derived as far as possible.

The GPS accuracy is below 1 m in position and about 0.05 m s^{-1} in speed. The present wind measurements procedure leads to uncertainties in boat speed about 0.11 m s^{-1} upwind and 0.23 m s^{-1} downwind. These values include sensors accuracies and interpolation errors. The current and the waves effects were also taken into account in the simulator. The current effect leads to uncertainty about 0.06 m s^{-1} in boat speed, based on the uncertainty of the public data provided by the SHOM, tide calculations, and time interpolation. The waves were not measured and some hypotheses were made in order to properly feed the IMS model from Claughton (1999). Since the sailing area was very sheltered from waves, it was assumed that the IMS model would lead to underestimate boat speed. On the contrary, neglecting waves would provide overestimated boat speed. Between these two extremes, it was rather crudely decided to retain a median value which equilibrates the upwind loss and the downwind gain in boat speed from waves effect, for the presented results such as those in Fig. 10. The associated uncertainty is about 0.07 m s^{-1} in speed boat. The effect of the ability of the real crew compared to the perfect simulated one remains an open issue.

Under the assumption the previous uncertainties are standard deviations under Gaussian assumptions, the global combination of these leads to standard deviations in boat speed of about 0.15 m s^{-1} upwind and 0.25 m s^{-1} downwind.

3.2. Dynamics simulations validation steps

The leading idea of the validation step is to perform comparisons between simulations and measurements with the same initial conditions. Thus, initial location, attitude, angular rate and velocity measured by the high resolution GPS DG16 sensor and the inertial unit MT9 from Xsens were taken as input data for the dynamic simulation.

3.2.1. Turning tests without sails

The yacht without sails was towed at a given and constant velocity between 5 and 6 knots before towing release. Once released, rudder angle was set to 50° till the end of the turning test. Turning results between simulation and yacht trajectory are shown in Fig. 8.

Note that the yacht velocity decreases quickly once released and that the trajectory is strongly impacted by the current of the sea and the windage. These kinds of effects were taken into account by the simulation that exhibits a very satisfying prediction for the first 360° turn. However, prediction of the second loop is much less satisfying. This mismatch was unfortunately predictable in case of very slow velocities since the yacht can, in that case, easily be disturbed in a chaotic manner by the waves for instance. As these disruptions are random phenomenon they were not taken into account in the modelling.

3.2.2. Tacking tests

Simulation capability was checked on real tacking tests, from starboard to portside tack. Same initial conditions as for the sea test were used for the simulation and the only governing parameter was the rudder angle. As shown in Fig. 9, velocity predicted by the simulation appears to be in good agreement with the data. Especially, the increase of velocity at the beginning of the tacking step was almost well predicted. This increase was certainly due to the location of the GPS sensor on the boat. In fact, the sensor was fixed at the stern of the boat. During the tacking the boat rotates around a vertical axis near the keel. This rotation combined with

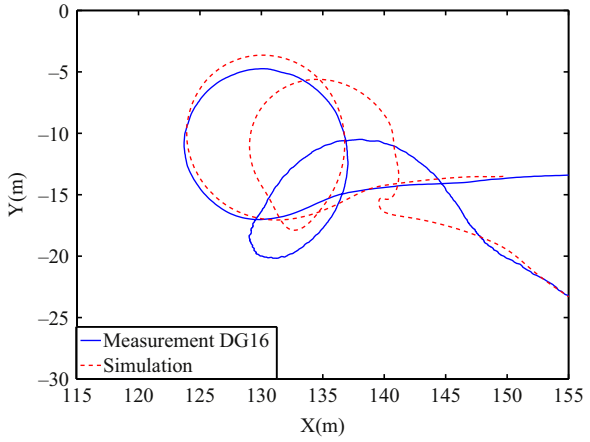

Fig. 8. Turning test results, without sail.

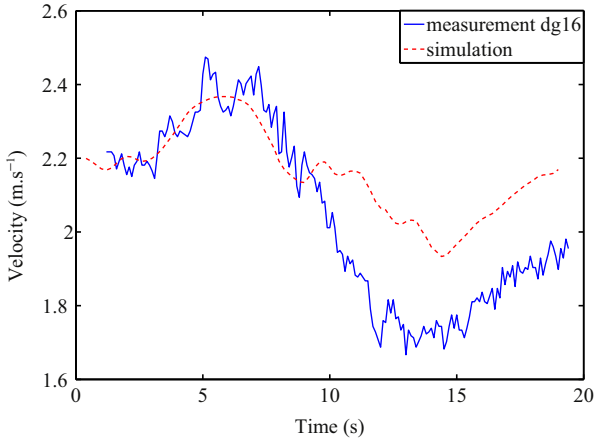

Fig. 9. Yacht velocity prediction during a tacking.

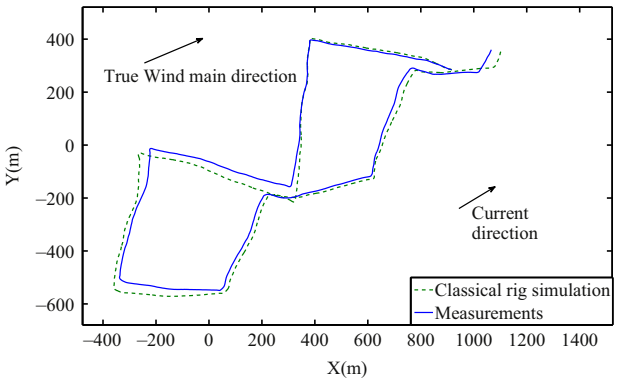

Fig. 10. Sailing Yacht trajectory prediction.

the GPS location on the boat leads to an increase of the velocity measured by the GPS sensor. As the GPS sensor location on the boat was taken into account for the simulation, the rotation effect on velocity could be predicted. However, velocity loss predicted at tacking exit is lower than what was observed (i.e. at tacking exit, the predicted velocity is higher than the measured one). At this stage it is difficult to explain this difference which could be due to crew motion effects, swell effects, manoeuvrability or aerodynamic models set into the simulation. Note that virtual crew trims the sails instantly in the simulation. Moreover flapping of the sails is not modelled in the dynamic VPP. However, this would not affect further kite rig simulation since tacking under kite power does not contain any flapping phenomenon.

3.2.3. *Sailing trajectory tests*

Turning and tacking tests have demonstrated a rather satisfying prediction ability of the simulator, in agreement with the physics observed. Even if some gap is observed at tacking exit, the trend is kept. The next and final validation step was to perform comparisons between simulation and data collected on a typical sailing trajectory. Fig. 10 shows results obtained for a trajectory composed by classical upwind and downwind legs.

The pilot of the simulated boat is only controlled by the measured relative wind angle at each time step. Trajectories for sailboat with a classical rig between the simulation and the measurements are in a very close agreement during the first upwind port leg and, after the first tacking, during two thirds of the second upwind starboard leg. After that, the real boat suddenly loses speed for an unknown reason. Therefore, the simulated trajectory deviates significantly from the measured one. Indeed, since the simulated boat is controlled by the measured relative wind angle, the loss in velocity necessarily results in an increase of the true wind angle to maintain the same relative wind angle. At the beginning of the third leg, a gap is observed and stays almost constant up to the end of the upwind leg.

At the first, and at the last downwind leg, the simulated yacht is faster than the real one. These phases correspond to the hoisting and the lowering of the spinnaker. Nevertheless one can reasonably consider that simulation results are in rather satisfying agreement with real sea trials. This enables therefore an acceptable validation of the simulator. Consequently, the simulator was extended to the case of kite propulsion and results are discussed in the next section.

4. Results

The optimization method described in Section 2.6 was used to obtain the velocity polar of the class 8 yacht towed by the kite described in Section 2.4 for a true wind velocity of 3 m s^{-1}. The kiteboat performances are then compared to the same yacht with a classical rig.

4.1. *Velocity polar diagrams $V_s(\beta_{WT})$*

The performance of a boat towed by kite can be assessed by its velocity for each true wind angle. Consequently, a boat velocity is first postulated which enables the required tethers tension calculation. Corresponding flying configuration is searched thanks to the optimization loop. Especially, boat drag and lift norms are equal to the projection of tethers tension T on $\mathbf{x}_F$ and $\mathbf{y}_F$ respectively. At this stage, corresponding new boat velocity and drift angle are calculated. The velocity is injected at the beginning of the optimization loop until convergence. The polar curve of the boat towed by a kite was obtained for static, vertical and horizontal dynamic flights as presented in Fig. 11. The use of these polar diagrams enables the determination of the flight configuration that provides the best upwind and downwind Vmg with corresponding true wind angles. Two optimal flight trajectories correspond to these two angles: a vertical dynamic flight for the upwind case (shown in Fig. 1) and an horizontal dynamic flight for the downwind case as shown in Fig. 11. The upwind Vmg is equal to 1.62 m s^{-1} with a true wind angle of 49° and a boat velocity of 2.47 m s^{-1}. The downwind Vmg is equal to 2.91 m s^{-1} with a true wind angle of 170° and a boat velocity of 2.95 m s^{-1}. Only these two optimal configurations were calculated and the best was retained. This allows the plot of final velocities polar diagrams for the kite towed boat as displayed in Fig. 11.

The discontinuity observed on the classical rig plot is due to the use of a spinnaker for relative wind angles of more than 80° (i.e. approximately 110° in true wind angle). In this configuration the classical rig surface is about 70 m^2 while the kite surface remains 35 m^2.

Fig. 11 clearly demonstrates that in case of a dynamic flight kite propulsion definitely performs much better than the classical rig, even with a spinnaker and a doubled total surface of 70 m².

This is also confirmed by apparent wind plots as shown in Figs. 12 and 13 where apparent wind seen by the kite is higher for upwind (at least +100%) and downwind (at least +200%) conditions. Consequently, apparent wind applied to the kite rig in downwind conditions, which is almost 3 times higher than for

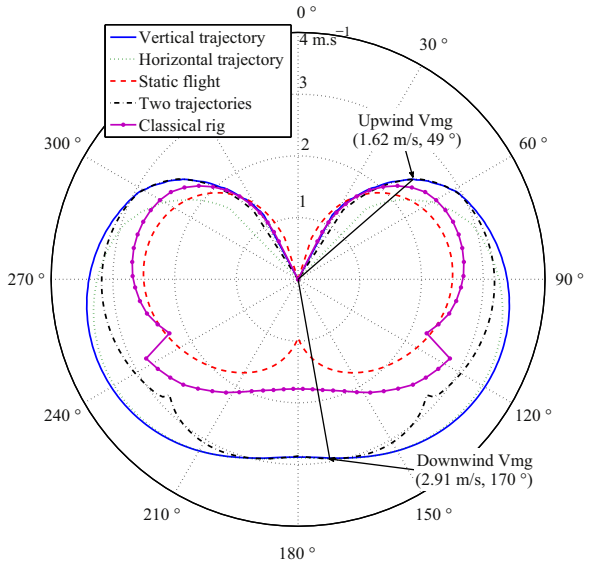

Fig. 11. Velocity polar diagrams versus true wind angle with U_{10}=3 m s^{-1}. (For interpretation of the references to color in this figure, the reader is referred to the web version of this article.)

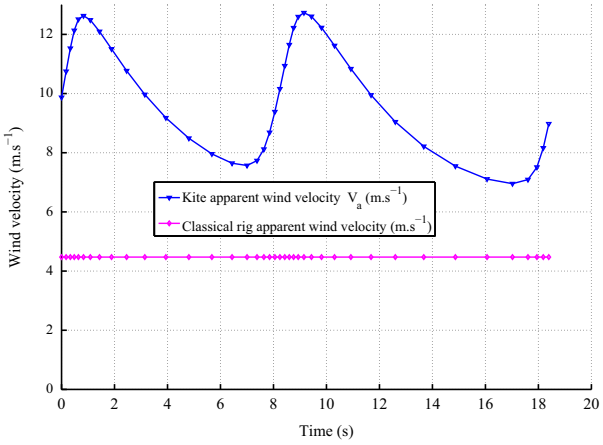

Fig. 12. Apparent wind evolution along an 8 shaped trajectory for a vertical dynamic flight in upwind conditions, for the class8 yacht and 3 m s^{-1} true wind.

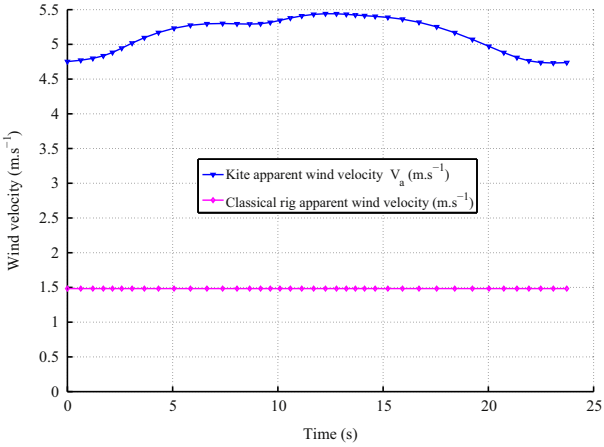

Fig. 13. Apparent wind evolution along an 8 shaped trajectory for an horizontal dynamic flight in downwind conditions, for the class8 yacht and 3 m s^{-1} true wind.

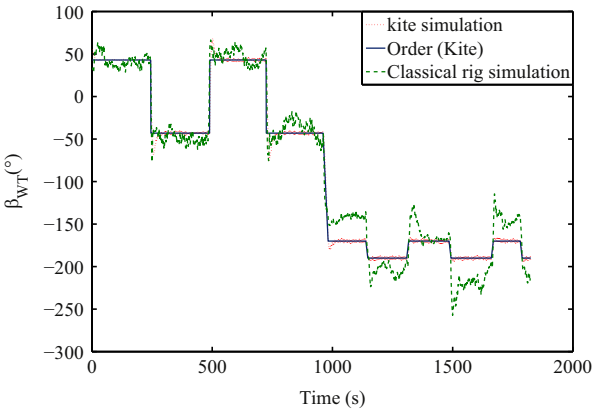

Fig. 14. True wind angle for kite and classical rig simulations. (For interpretation of the references to color in this figure, the reader is referred to the web version of this article.)

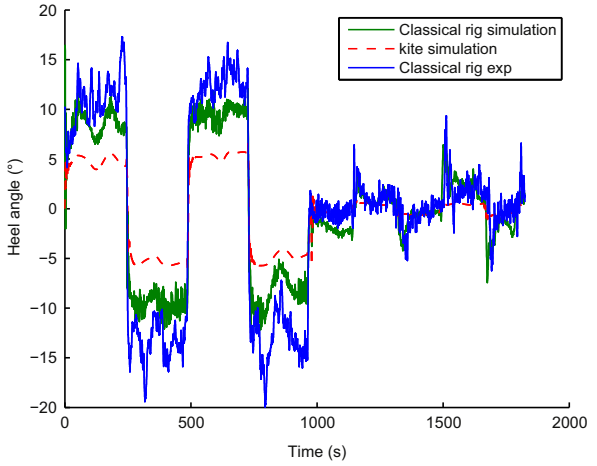

Fig. 15. Time evolutions of experimental and numerical heel angles with classical rig and kite.

the classical rig leads logically to large speed increase as shown in Fig. 11.

4.2. Comparison between classic rig and kite propulsion on a typical sailing trajectory

The same configuration as for validation of the classical rig yacht simulation was used for the comparison between a kite towed boat and the same boat with a classical rig. The aerodynamic module for a classical rig boat developed by Claughton (1999) was replaced by the module for propulsive force generated by the kite presented in the second section.

Relative wind angle β_{WR} measured during sea trials appears to be not relevant to pilot a kite towed boat. Indeed, since boat velocities differ significantly, optimum working points have very different relative wind too. It was therefore chosen to pilot the kite towed boat according to true wind angle, in order to have similar trajectories. Manoeuvres were synchronized with sea trials ones. True wind angle orders given for the kite towed boat are shown in Fig. 14 and were deduced from velocity polar diagrams (Fig. 11) data for upwind and downwind Vmg. The dotted line exhibits sometimes some small gaps which are related to tacking simulation. The green dotted line denotes the true wind angle seen by the classical rig boat. The rough shape observed is related to wind measurement dispersion. Furthermore, if upwind angle reached by the kite towed boat and the classical rig boat are close, it is absolutely not the case for downwind conditions since kite propulsion enables a higher downwind efficiency thanks to the dynamic flight mode.

Fig. 15 presents the time evolutions of the heel angles measured during the experimental test and resulting from the numerical simulations with kite and classical rig. The classical rig simulation curve presents a noise, because the true wind angle order chosen for the numerical simulation comes from the measurements as shown in Fig. 14. It is interesting to check here that despite the greater forces produced by the kite, the heel angle is smaller compared to the classical rig. However it can be noticed that, just before 1000 s, the heel angle of the kite simulation shows stronger oscillation amplitude than for the classical rig simulation. This is when the boat bore away from the upwind leg to the downwind leg. The orientation of the 8-shaped kite trajectory then changed from vertical to horizontal and went to full window where power and speed are maximum. There is here a dramatic increase of towing tension at that time as shown in Fig. 16.

Fig. 16 shows mean load polar evolutions along the 8 shape trajectory used for the dynamic flight. Maximum load observed during the 8 shape trajectory can reach 180% of the mean load in upwind conditions, whereas it only reaches 110% in case of downwind conditions. It is definitely the downwind conditions that trigger maximum load to consider for the design. This leads then to the question of the structural compatibility of existing yacht to use kite rigs. Of course, this is strongly also related to

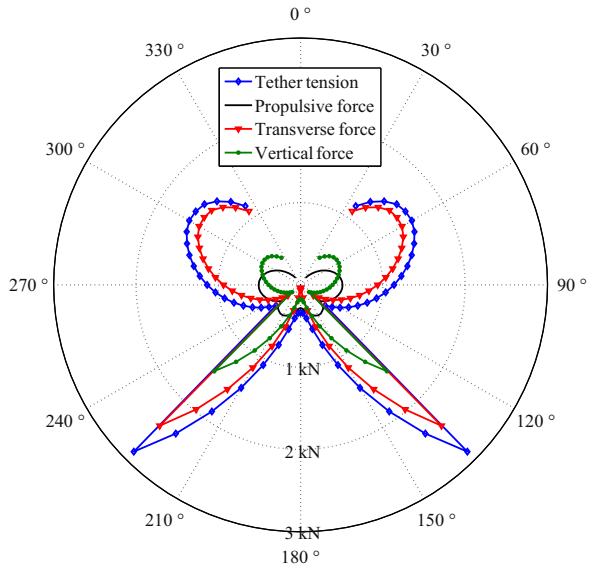

Fig. 16. Polar diagrams versus the true wind angle of the numerical simulation of the attachment loads of the towing kite in the case of 8-shaped dynamic flight (V_{WT} 3 m s^{-1}).

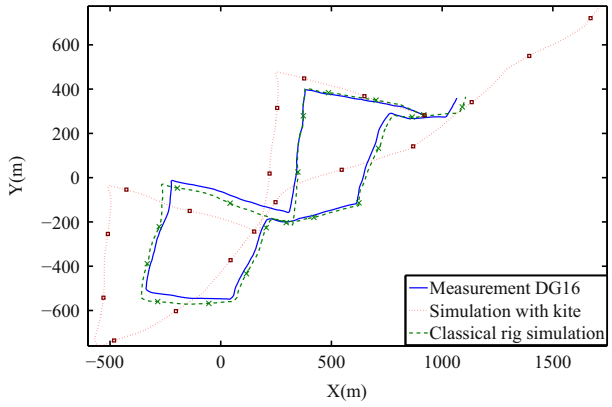

Fig. 17. Classical rig and kite comparison.

the kite area used. Anyway, this clearly requires a case by case dedicated structural analysis of the existing yacht, if added aftermarket.

A trajectory comparison is shown in Fig. 17 where markers were put each 100 s to highlight time evolution of each boat. It is clearly demonstrated that kite propulsion enables a significant upwind performance benefit which is even higher in downwind conditions. The analysis of the distance elapsed within 961 s shows that, by kite propulsion, the upwind Vmg reached is 1.86 m s^{-1} instead of 1.57 m s^{-1} by classical rig (1.54 m s^{-1} during sea trials). In a same manner, the analysis of the distance elapsed between 990 s and 1820 s shows that the downwind Vmg reached is 3.24 m s^{-1} by kite instead of 2.02 m s^{-1} by the classical rig (1.94 m s^{-1} during sea trials). These results are consistent with Fig. 11 polar diagrams according to the fact that average wind speed during sea trials was 3.6 m s^{-1}.

5. Discussion

Although the comparison between classical rig and kite propulsion clearly demonstrated that kite propulsion enables significant performance benefits, the kiteboat modelling could be improved by taking into account some parameters more precisely.

It can be seen in Fig. 11 that, excepted for very small true wind angles, the classical rig performed better than the kite static flight. This can be explained by the fact that the trim of a classical rig allows to reach more important forces by increasing the draft of the sails. An additional fundamental explanation about performance differences between classical rig and kite static flight might be given by the lift coefficient that, according to IMS (Claughton, 1999), can reach values of 1.5–1.7 for sails whereas a value of 0.776 was measured by Dadd (Dadd et al., 2010, 2011) on the kite. On the other hand the kite provides a better lift to drag ratio that allows to reach closer hauled true wind angles and probably a better upwind performance in stronger wind conditions. In addition an optimization on the trim angle of attack which is not achieved in the present study could be done to make better results in light wind condition or wider true wind angles.

The static flight has been studied and it appears to be efficient only for small wind angles. Nevertheless these conditions are frequently encountered in case of fast yachts. The static flight case would also enable much easier kite operation. In such cases, the use of a static flight would avoid issues related to kite size change manoeuvres which are weak points for kite towed systems.

Fig. 15 shows pretty good agreement for heel angle prediction and measurements for the classical rig case. On the other hand, heel angle for kite simulation is lower than for classical rig. This result is consistent since for a given yacht's righting moment (i.e. same heel angle), the sailing side force from the classical rig is lower than the one generated by the kite rig. Indeed, kite line of action is driven by its tether direction which tows upwards and close to the deck rather than downwards, normal to the heeled rig, through a point above the deck at the centre of effort of the sails. Thus, in the current case study and for the same true wind conditions, heel angle is found lower in the case of kite rig propulsion. Moreover for the same upwind conditions, kite sailing side force would be higher inducing therefore higher drift angle.

The results presented for dynamic flight are dependent on trajectory size. Nevertheless, the optimal trajectory size remains difficult to define. The smaller the trajectory is, the more efficient it is in terms of tether tension as shown by Dadd et al. (2011). However, it was experimentally observed that tethers tension and kite velocity decrease in turning stages at the extremities of an 8-shaped trajectory. Therefore, small trajectories will lead to higher rotation velocities in the curved parts of the trajectory. In these parts, the aerodynamic characteristics of the kite are modified due to the asymmetry of the loading. A kite's overall lift to drag ratio decreases as a function of rotation velocity was also modelled in a simple way in a previous study (Leloup et al., 2012). This aspect will have to be addressed in future works to enhance the optimal trajectory size computation.

6. Conclusion

Results have clearly demonstrated the significant benefit that would be provided by kite propulsion compared to classical rig propulsion. As shown in Fig. 11, the most important benefit is provided by dynamic flight cases for the kite. If we assume now as a first simple approach that, on one hand kite propulsive force and required vessel propulsive forces are linearly dependent on kite area and vessel square velocity, and on the other hand that Vmg velocity is more or less proportional to vessel velocity, one finds that kite area ratio is proportional to square boat velocity ratio for two cases of kite area considered. Consequently, kite area corresponding to the same velocity as for the classical rig, is given by initial kite area divided by square velocity ratio. In this study, the use of the same classical rig area as for kite propulsion led to square Vmg ratio increase from 1.57 m s^{-1} to 1.86 m s^{-1} (square

increase of 40%) and in and downwind conditions from 2.02 m s^{-1} to 3.24 m s^{-1} (square increase of 250%). This leads then to a 25 m² area in upwind conditions (35/1.4=25 m²) and to a 10 m² area in downwind conditions (35/3.5=10 m²). Same performance as for classical rig can be reached for significant smaller kite sizes which is also a benefit, from practical considerations such as handling, launch and recovery for instance.

In accordance with Dadd et al. (2010, 2011) initially proposed idea for vertical flight, this study clearly demonstrated the advantage of vertical flight for upwind conditions. This interesting configuration seems to have been forgotten probably because of few kite towed ship studies existing in the literature in comparison with kite powered electricity supply studies (Loyd, 1980). On the other hand, this study has also highlighted the benefit of static flight case for small wind angles. The static flight case would also ensure benefits for reinforcing wind conditions and vessel stability issues. In such cases, the use of kite static flights should avoid issues related to kite size changes manoeuvres which are weak points for kite towed systems.

Although results were set on experimentally validated models, they are subjected to control command units that must be able to ensure reliable optimal flight trajectories. Required electrical supply for such control command units must still be estimated. Questions about woven fabrics durability and aerodynamic characteristics changes in tight turns remain open ended. These issues are strongly related to the increase of kite area, especially for merchant vessels application of kite propulsion. The question of kite use as auxiliary propulsion device for merchant vessels is currently investigated by the authors. Additionally to dynamic flight, static flight benefit, which does not match with an optimal working point for the sailing yacht investigated here, should be more visible for merchant vessels.

Acknowledgements

The authors of this paper are grateful to the French ministry of defence and the OCEA Company for their financial support. In addition we would like to thank Ecole Nationale de Voile et des Sports Nautiques, Ecole Centrale de Nantes, IUT de Nantes and the companies Thales and CADDEN for their support during the sea trials.

References

Argatov, I., Rautakorpi, P., Silvennoinen, R., 2009. Estimation of the mechanical energy output of the kite wind generator. Renew. Energy 34 (6), 1525–1532.

Bosch, A., Paolo Tiso, Schmehl R., Rixen, D., 2014. Dynamic nonlinear aeroelastic model of a kite for power generation. J. Guid. Control, Dyn. 31 (1), 81–93.

Breukels, J., 2011. An Engineering Methodology for Kite Design (Ph.D. Thesis). Delft University of Technology ⟨http://www.kitepower.eu/publications.html⟩ (accessed July 2013).

Claughton, A. Developments in the IMS VPP Formulations, In : Fourteenth Chesapeake Sailing Yacht Symposium. Annapolis, Maryland. 1999. pp. 1–20.

Costello, S., Francois, G., Bonvin, D., 2013. Real-Time Optimization for Kites. In: 5th IFAC International Workshop on Periodic Control Systems (PSYCO'2013).

Dadd, G.M., Hudson, D.A., Shenoi, R.A., 2010. Comparison of two kite force models with experiment. J. Aircr. 47 (1), 212–224.

Dadd, G.M., Hudson, D.A., Shenoi, R.A., 2011. Determination of kite forces using three-dimensional flight trajectories for ship propulsion. Renew. Energy 36 (10), 2667–2678.

Dadd, G.M., 2013. Kite Dynamics for Ship Propulsion (Ph.D. thesis). University of Southampton.

de Wachter, A., 2008. Kiteplane flight dynamics (M.Sc. thesis). Delft University of Technology.

de Groot, S.G.C., 2010. Modelling the Dynamics of an Arc-Shaped Kite for Control Law Design (M.Sc. thesis). Delft University of Technology ⟨http://repository.tudelft.nl/view/ir/uuid%3A5f493a5d-da9c-457f-be28-799a63cb42d9/⟩.

Erhard, M., Strauch, H., 2013a. Theory and experimental validation of a simple comprehensible model of tethered kite dynamics used for controller design (Chapter 8). In: Ahrens, U., Diehl, M., Schmehl, R. (Eds.), Airborne Wind Energy. Springer, Berlin Heidelberg,http://dx.doi.org/10.1007/978-3-642-39965-7_8.

ITTC Symbols and Terminology List. International Towing Tank Conference. Version 2011.

Fagiano, L., 2009. Control of Tethered Airfoils for High-Altitude Wind Energy Generation (Ph.D. thesis). Royal Turin Polytechnic (accessed July 2013).

Leloup, R., Roncin, K., Bles, G., Leroux, J.B., Jochum, C., Parlier, Y., 2012. Estimation of the effect of rotation on the drag angle by using the lifting line method: application to towing kites for auxiliary propulsion of vessels. In: 13èmes Journées de l'Hydrodynamique. Chatou, France. URL : ⟨http://website.ec-nantes.fr/actesjh/images/13JH/Annexe/13jh-s04.htm⟩ (accessed July 2013).

Leloup, R., Roncin, K., Bles, G., Leroux, J.B., Jochum, C., Parlier, Y., 2013a. Estimation of the lift-to-drag ratio using the lifting line method: application to a Leading Edge Inflatable kite. In: Ahrens, U., Diehl, M., Schmehl, R. (Eds.), Airborne Wind Energy. Berlin Heidelberg, Springer http://dx.doi.org/10.1007/978-3-642-39965-7_19 (Chapter 19).

Leloup, R., Roncin, K., Bles, G., Leroux, J.-B., Jochum, C., Parlier, Y., 2013b. A novel modelling for performance assessment of kites as auxiliary propulsion device for merchant ships. In: Proceedings of the 16th International Conference on Computer Applications in Shipbuilding. Busan, South Korea.

Loyd, M.L., 1980. Crosswind kite power (for large-scale wind power production). J. Energy 4 (3), 106–111.

Maneia, G.M., 2007. Aerodynamic Study of Airfoils and Wings for Power Kites Applications (M.Sc. thesis). Politecnico di Torino ⟨http://maneia.com/doc/MasterThesisManeia.pdf⟩ (accessed July 2013).

Naaijen, P., Koster, V., Dallinga, R.P., 2006. On the power savings by an auxiliary kite propulsion system. Int. Shipbuild. Prog. 53 (4), 255–279.

Naaijen, P., Shi, W., Kherian, J.G., 2010. Assessing the fuel saving by using auxiliary wind propulsion from traction kites. Ship design and operation for environmental sustainability. The Royal Institution of Naval Architects (RINA), London.

Roncin, K., Kobus, J.M., 2004. Dynamic simulation of two sailing boats in match-racing. Sports Eng. 7 (3), 139–152.

Roncin, K., Kobus, J.M., Iachkine, P., et al., 2005. Méthodologie pour la validation du simulateur de voilier par des essais en mer, une première tentative. In : Workshop Science-Voile. pp. 1–10.

Terink, E., 2009. Kiteplane Flight Dynamics (M.Sc. thesis). Delft University of Technology.

Wellicome, J.F., Wilkinson, S., 1984. Ship Propulsion Kites: An Initial Study. University of Southampton Department of Ship Science, Faculty of Engineering and Applied Science. Tech. Rept. SSSU 19.